J Mater Sci: Mater Med (2012) 23:1835–1847
DOI 10.1007/s10856-012-4660-0

Structural and biomechanical characterizations of porcine myocardial extracellular matrix

Bo Wang · Mary E. Tedder · Clara E. Perez · Guangjun Wang · Amy L. de Jongh Curry · Filip To · Steven H. Elder · Lakiesha N. Williams · Dan T. Simionescu · Jun Liao

Received: 13 January 2012 / Accepted: 23 April 2012 / Published online: 15 May 2012

Abstract Extracellular matrix (ECM) of myocardium plays an important role to maintain a multilayered helical architecture of cardiomyocytes. In this study, we have characterized the structural and biomechanical properties of porcine myocardial ECM. Fresh myocardium were decellularized in a rotating bioreactor using 0.1 % sodium dodecyl sulfate solution. Masson's trichrome staining and SEM demonstrated the removal of cells and preservation of the interconnected 3D cardiomyocyte lacunae. Movat's pentachrome staining showed the preservation of cardiac elastin ultrastructure and vascular elastin distribution/alignment. DNA assay result confirmed a 98.59 % reduction in DNA content; the acellular myocardial scaffolds were found completely lack of staining for the porcine α-Gal antigen; and the accelerating enzymatic degradation assessment showed a constant degradation rate. Tensile and shear properties of the acellular myocardial scaffolds were also evaluated. Our observations showed that the acellular myocardial ECM possessed important traits of biodegradable scaffolds, indicating the potentials in cardiac regeneration and whole heart tissue engineering.

B. Wang · C. E. Perez · G. Wang · F. To · S. H. Elder · L. N. Williams · J. Liao (✉)
Tissue Bioengineering Laboratory, Department of Agricultural and Biological Engineering, Computational Manufacturing and Design, CAVS, Mississippi State University, 130 Creelman Street, Room 222, Starkville, MS 39762, USA
e-mail: jliao@abe.msstate.edu

M. E. Tedder · D. T. Simionescu
Department of Bioengineering, Clemson University, Clemson, SC, USA

A. L. de Jongh Curry
Department of Biomedical Engineering, University of Memphis, Memphis, TN, USA

1 Introduction

Myocardial infarction (MI) and heart failure are the leading causes of mortality world-wide, [1] which are characterized by progressive ventricular chamber dilatation, tissue fibrosis, and wall thinning of the infarct region [2–4]. Recent studies on MI treatment are focusing on cell therapies (myoblast/stem cell injection) [5], intramyocardial gene transfer [6], and cardiac repair with tissue engineered constructs [5, 7, 8]. Among the treatments, tissue engineering strategies have recently attracted much attention due to the potential to restore cardiac function using viable tissue constructs [9–11].

The goal of cardiac tissue engineering is to fabricate tissue constructs that can restore basic cardiac functions by integrating cellular components with scaffolds that serve as a structural guide [12–15]. Various cell types, such as stem cells (bone marrow stem cells, umbilical stem cells, embryonic stem cells), multipotent adult progenitor cells, fetal cardiomyocytes, smooth muscle cells, and dermal fibroblasts, have been investigated as cell sources for recellularization [16–20]. Another key challenge for cardiac tissue engineering is to identify the most suitable scaffold materials, which can provide optimal structural support and guide for cell reseeding, proliferation, differentiation, and functional integration. Two major approaches have been investigated intensively to indentify ideal scaffolds: one is to use synthetic biodegradable material and another is to use tissue-derived acellular scaffolds [10, 11] [4, 16, 17].

Synthetic biodegradable material such as polyglycolic acid (PGA), polylactic acid (PLA), poly ester (urethane urea) (PEUU), poly(caprolactone) (PCL), poly(ethylene oxide) (PEO), poly(vinyl alcohol) (PVA), and poly(glycerol sebacate) have been used as scaffold materials [21–27]. The advantages of polymeric materials include biodegradability

and reproducibility with certain material and structural properties [28, 29, 21]. However, the synthetic polymeric approach faces challenges such as inflammatory and immune responses, mismatched mechanical properties, nonpliability, and control of degradation rate [26] [30, 31].

Recently, acellular scaffolds derived from native tissues have gained attentions in the field of tissue engineering/regeneration [32–40, 26]. The major advantage of the decellularization approach is that the mechanical and biological properties of the extracellular matrix (ECM) are well preserved [41–43, 35]. As an milestone study, Ott et al. showed a revitalized beating rat heart by recellularizing a decellularized intact rat heart with cardiac and endothelial cells [44]. Ott et al. found that the decellularization was able to thoroughly remove cells/cell debris and retain perfusable vascular architecture, competent acellular valves and intact chamber geometry [44]. A pump function similar to 2 % of adult or 25 % of 16 week fetal heart was observed under a physiological load and electrical stimulation. Ott's study on rat hearts revealed that acellular myocardial ECM itself might provides the most optimal ECM environment for cardiac tissue engineering. To further assess the potential of acellular myocardial scaffolds as a tissue engineered (TE) template at a larger scale, we investigated the decellularized porcine myocardium, [45] demonstrating that the native 3D cardiomyocyte lacunae and ECM networks were preserved and the acellular porcine myocardial scaffold showed potential in supporting cell reseeding, cell differentiation, and endothelialization of vasculature channels [45]. Moreover, a recovery of mechanical properties was also observed along with the tissue culture time [45].

Currently, two lines of research are emerging around myocardium decellularization: one is to harness the potential of acellular myocardial scaffolds as a template for cardiac patch tissue engineering, as exemplified by Wang's study on porcine myocardium [45] and Godier-Furnemont's study on human myocardium; [46] another approach, currently undertaken by Badylak et al. and Taylor et al., is to scale up whole heart tissue engineering from rat heart to pig heart [47, 48]. Apparently, both patch-level and whole heart level applications require better understanding of the structural and biomechanical properties of the myocardial ECM [49, 47, 50].

Myocardial ECM is an intriguing network that mediates complex muscle fiber architecture and maintains unique cell to cell interconnections [51–54]. Composed of collagen (type I and III) fiber network, elastin, proteoglycans, and glycosaminoglycans [51–54], myocardial ECM provides important functions in maintaining structural integrity, tethering myocytes and mediating their contraction/relaxation, and preventing excessive stretching [55–57]. Being able to obtain acellular myocardial scaffolds with well preserved ECM components and 3D architecture offers an opportunity to examine the myocardial ECM in great detail.

In this project, we carried out structural and biomechanical characterizations on the acellular myocardial scaffolds. The assessments of the acellular scaffold enable us to better understand the intrinsic structural and mechanical characteristics of myocardial ECM. The knowledge gained in this research will (i) provide a baseline for cardiac tissue engineering that either partially or wholly utilizes the acellular porcine myocardial scaffolds and (ii) serve as a reference for polymeric based cardiac scaffold design.

2 Materials and methods

2.1 Preparation of acellular myocardial scaffolds

Thirty fresh porcine hearts were obtained from juvenile pigs ($\sim$6-month old) from a local abattoir and transported to the laboratory in PBS on ice. Myocardium square ($20 \times 20 \times 3$ mm) or myocardium strip ($30 \times 10 \times 3$ mm) was dissected from the middle region of the anterior left ventricular wall of the porcine heart. Square samples were used for histological, structural, and biochemical characterizations, and the strip samples were used for uniaxial and shear testings. For the square samples, one edge was aligned along with the muscle fiber preferred direction (PD) that was determined by the overall fiber texture and heart anatomy. For the strip samples, the long edge either aligned along with the muscle fiber PD direction or aligned along with the cross fiber preferred direction (XD).

A frame-pin supporting system was designed to better maintain tissue macrogeometry during decellularization (Fig. 1). Briefly, four corners of the myocardium sample were perforated with four 27G $\times$ 31/2″ BD Quincke Spinal Needles, which were then mounted onto custom made rectangular plastic frames. The myocardium was then decellularized in a rotating bioreactor using 0.1 % sodium dodecyl sulfate (SDS) (Sigma) with 0.01 % trypsin (VWR), 1 mM phenylmethylsulfonylfluoride (PMSF, protease inhibitor) (Sigma), 20 μg/ml RNase A (Sigma) and 0.2 mg/ml DNase (Sigma) at room temperature for 2.5 weeks. Ten-minute ultrasonic treatment (50 Hz, Branson) was applied each day; the solution was changed every two days to avoid contamination and tissue deterioration.

2.2 Morphology, histology and SEM

For estimating the dimensional changes, the thickness and surface area of native myocardium samples were measured using a caliper and the digital picture of the samples, respectively. After decellularization, the thickness and surface area of the acellular myocardial scaffolds were

Fig. 1 The frame-pin supporting system was found to preserve tissue morphology well in the decellularization procedure. The porcine myocardium showed bright *white color* after 2.5 week SDS treatment, indicating that decellularization was achieved. **a** Sample morphology after 3 day decellularization; **b** sample morphology after 2.5 week decellularization (Color figure online)

immediately measured in order to compare the dimensional alterations.

For histological analysis, samples were fixed in 2 % paraformaldehyde in PBS at room temperature for 2 h, dehydrated with graduated concentrations of ethanol and embedded in paraffin. Cross-sections of the myocardium were cut to 5 μm thick. To elucidate changes in tissue components, Masson's trichrome staining and Movat's pentachrome staining were used to identify cardiomyocytes, collagen network, elastin, and proteoglycans. Stained tissue sections were imaged using bright field microscopy (Nikon EC600). Polarizing light imaging was also taken to reveal the light extinguishing patterns of collagen network in both the acellular myocardial scaffolds and the native myocardium.

Scanning electron microscope (SEM), capable of showing 3D topography, was used to observe the cross section of the acellular scaffolds and the native myocardium. After fixation with 2.5 % glutaraldehyde for 24 h, the samples were dehydrated in a graded ethanol series. The samples were then processed with critical point drying (Polaron E 3000 CPD), sputter coated with gold–palladium, and observed with SEM (JEOL JSM-6500 FE-SEM).

2.3 DNA assay and *Griffonia simplicifolia* (GS) lectin immunohistochemistry

To test for the completeness of decellularization, both the native myocardium and the acellular scaffolds were weighed wet; DNA was extracted and purified with a specific kit (Qiagen, Valencia, CA). The amounts of DNA were quantified by reading absorbance at 260 nm, and quantities of DNA were normalized to the wet weight and expressed as ng/mg. To detect Gal α 1-3Gal (α-Gal), the main porcine antigen responsible for acute rejection of xenotransplants, biotinylated *G. simplicifolia* (GS) lectin immunohistochemistry was performed, followed by ABC-peroxidase complex and DAB detection with haematoxylin counterstaining [58, 59].

2.4 Differential scanning calorimetry, water content, and collagen stabilization studies

Acellular myocardial scaffolds were subjected to differential scanning calorimetry (DSC, model 131 Setaram Instrumentation, Caluire, France) to determine the thermal

denaturation temperature (T_d). Specimens were tested at a heating rate of 10 °C/min from 24 to 100 °C in a N_2 gas environment ($N = 4$). T_d is defined as the temperature at the endothermic peak and is a well-known indicator of degree of collagen crosslinking [60].

Water content was calculated as the percentage weight difference between wet and dry samples that was normalized to the wet weight. Both the native myocardium and the acellular scaffolds were cut into small pieces ($3 \times 3 \times 3$ mm^3) and the surfacing moisture was absorbed using filter paper. After measuring the wet weight, all the samples were put into a Freeze Dryer System (Cole-Parmer, Illinois) at −54 °C. After samples were totally dried, the dry weights were immediately measured ($N = 24$ for each group).

To assess degradability of acellular myocardium scaffolds, collagenase treatment was applied as an accelerated degradation model [60]. After lyophilization, the dry weight of the samples were recorded (range from 10 to 15 mg) and samples were then incubated in 1 mL collagenase Type I (USB) solution (5 Units of collagenase/mL in 50 mM Tris buffer, 1 mM $CaCl_2$, 0.02 % NaN_3, pH = 7.8). At 3 and 7 days, samples ($N = 6$ per time point) were rinsed three times in ddH_2O by centrifugation at 12,000 rpm for 5 min, lyophilized, and weighed. Percent mass loss was calculated from the following equation: (scaffold weight before collagenase treatment - scaffold weight after collagenase treatment)/scaffold weight before collagenase treatment.

2.5 Mechanical characterizations

2.5.1 Uniaxial mechanical testing

Uniaxial mechanical properties of the acellular myocardial scaffolds were characterized with a uniaxial testing machine (Mach-1, Biosyntech, MN). Dogbone-shaped tissue strips were trimmed in a way that a group of samples were aligned along fiber-preferred direction (PD) and another group of samples were aligned along cross fiber-preferred direction (XD) ($N = 4$, grip-to-grip length: 20 mm, width: 5 mm). The samples were mounted with two stainless steel grips cushioned with emery paper. After 10 cycles of preconditioning at 10 % strain, tissue samples were loaded to failure at a ramp speed of 400 μm/s.

Engineering stress was calculated by normalizing the force to the initial cross-sectional area; engineering strain was computed by normalizing the displacement to the initial grip-to-grip distance (gauge length). The maximum tensile modulus was estimated by finding the tangent value of the linear region of the stress–strain curve using linear regression. Failure stress and failure strain were also determined from the stress–strain data. To assess energy dissipation in tissue loading and unloading, last cycle of preconditioning was used to estimate the tissue hysteresis, by normalizing the enclosed area of the loading and unloading curves (energy dissipation) to the area underneath the loading curve (energy input).

2.5.2 Shear testing

A pair of custom made shear plates was mounted onto the Mach-1 for shear mechanical testing on both the acellular myocardial scaffolds and the native myocardium. In the testing, tissue sample ($N = 4$ for each group), with PD direction aligned along with shear direction, was mounted between two shear plates by applying a minimum amount of cyanoacrylate glue. After ten cycles of preconditioning, sample was loaded to a shear strain level of 40 % (~10 kPa shear stress level for the native myocardium; ~400 Pa shear stress level for the acellular myocardial scaffolds). Shear stress was computed by normalizing the shear force to the contact area; shear strain was computed by normalizing the travel distance of shear plate to the sample thickness. All samples were tested in a PBS bath at 37 °C.

2.6 Statistical analysis

The experimental data were presented as mean ± standard deviation (STDEV). The Student's t test was applied for two-group comparison (SigmaStat 3.0, SPSS, Chicago, IL). The differences were considered statistically significant when $P < 0.05$.

3 Results

3.1 Morphological, histological, and SEM analyses

Consistent with our previous finding [45], after 2.5 week SDS treatment the porcine native myocardium (NM) showed bright white color of typical collagenous materials, indicating that decellularization was achieved (Fig. 1). The dimensional comparison of myocardium samples before and after decellularization demonstrated that the acellular myocardial scaffolds (AMS) decreased in thickness (NM vs. AMS: 2.70 ± 0.23 vs. 2.27 ± 0.38 mm, $P = 0.039$), were larger in surface area (NM vs. AMS: 520.13 ± 46.94 vs. 577.42 ± 44.51 mm^2, $P = 0.055$), and showed only a small degree of overall contraction (NM vs. AMS: 1403.25 ± 232.36 vs. 1314.74 ± 216.29 mm^3, $P = 0.510$) (Table 1; Fig. 7). The removal of cardiomyocytes was confirmed by Mason's trichrome staining, and the cardiomyocyte lacunae were found to be preserved, evidenced by cross-sectional and longitudinal histology (Fig. 2). The 3D topography of the acellular scaffolds further delineated the details of the well preserved

Table 1 Parameters from structural characterizations and water content measurement

	Thickness (mm)	Surface area (mm^2)	Volume (mm^3)	Pore size (μm)	Water content (%)
Native myocardium	2.70 ± 0.23	520.1 ± 46.9	1,403.25 ± 232.36	NA	77.99 ± 0.46
Acellular myocardial scaffolds	2.27 ± 0.38*	577.4 ± 44.5	1,314.74 ± 216.29	21.4 ± 16.8	90.21 ± 2.36*
P value	$P = 0.039$	$P = 0.055$	$P = 0.510$	NA	$P < 0.001$

* Indicates statistically significant difference between two groups ($P < 0.05$)

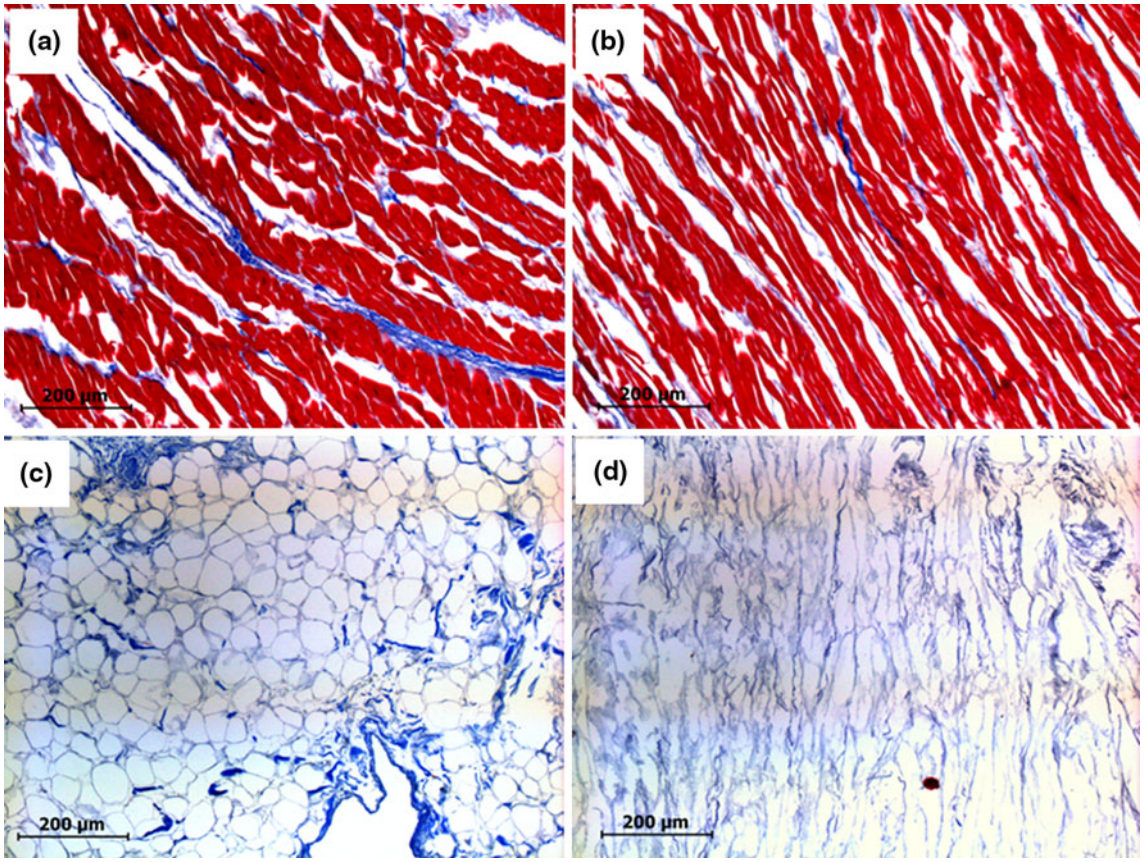

Fig. 2 Mason's trichrome staining showed well preserved cardiomyocyte lacunae. **a** Cross-section of the native myocardium; **b** longitudinal-section of the native myocardium; **c** cross-section of the decellularized myocardium; **d** longitudinal-section of the decellularized myocardium. *Red* cardiomyocytes, *blue* collagen (Color figure online)

cardiomyocyte lacunae, which were characterized by an array of interconnecting open pores (Fig. 3c, d). The average pore size estimated from the SEM images was 21.4 ± 16.8 μm. Note that the SEM topography of the native myocardium showed a dense morphology with muscle cells interlaced with myocardial ECM (Fig. 3a, b), very different from the topography of the acellular scaffolds (Fig. 3c, d).

Under polarizing light, the collagen scaffolds in the native myocardium showed light extinguishing phenomenon that were corresponding to collagen wavy pathways (Fig. 4a, b). In the acellular myocardial scaffolds, the light extinguishing phenomenon were found to be retained, implying the subtle collagen wavy pathway survived the decellularization procedure (Fig. 4c, d). The elastin structures in the acellular myocardial scaffolds were revealed by Movat's pentachrome staining (Fig. 5). Both vasculature elastin and cardiac elastin, with their subtle structural features, were retained after the decellularization (Fig. 5, arrows showing cardiac elastin). As shown in Fig. 5c, a circle of elastin lamina on the intima was observed, and the elastin fibers in the media and adventitia maintained certain alignment and distribution. Furthermore, the removal of the cellular contents (e.g., smooth muscle cells) in blood vessels were also evidenced in the Movat's staining (Fig. 5c).

3.2 DNA assay, porcine antigen characterization, DSC, and enzymatic resistance

Quantitative DNA analysis showed that the decellularized scaffolds had a 98.59 % reduction in DNA content

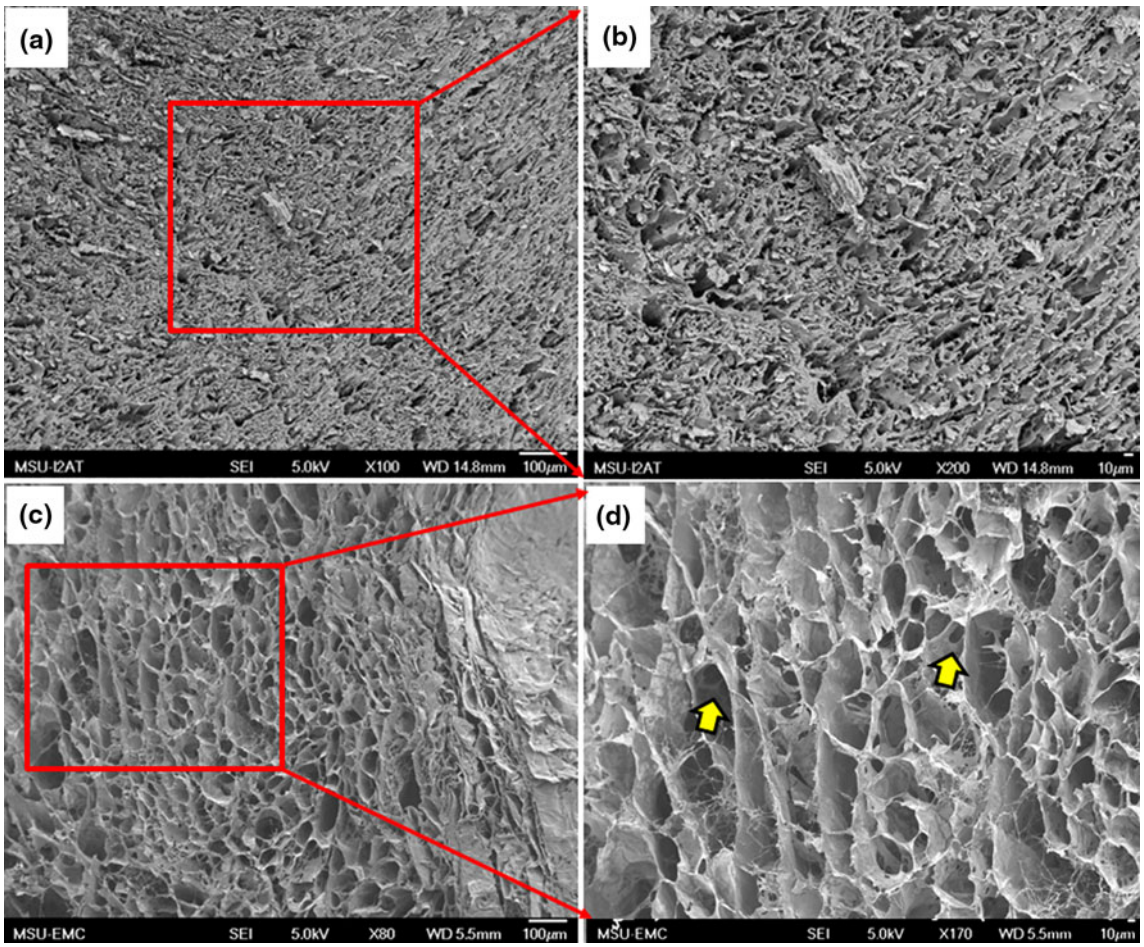

Fig. 3 **a** Cross-sectional view of the native myocardium revealed by SEM, **b** enlarged view. **c** Three-dimensional topography of the acellular myocardial scaffolds revealed by SEM; **d** enlarged view of the cross-section; *arrows* highlight the interconnecting openings inside the aligned cardiomyocyte lacunae

compared with the native myocardium (from 275.4 $\pm$ 31.7 to 3.9 $\pm$ 0.5 ng DNA/mg wet tissue). Results of α-Gal antigen staining showed that in the native porcine myocardium, α-Gal antigen (brown color) was associated with myocardial fibroblasts, cardiomyocytes and blood vessels, while in the acellular myocardial scaffolds, α-Gal antigen was completely absent (Fig. 6).

The DSC analysis found that the acellular myocardial scaffolds had a T_d value of 70.28 $\pm$ 1.39 °C, falling into the range of thermal denaturation temperature of typical collagenous scaffolds [61]. The collagenase treatment showed that the acellular myocardial scaffolds experienced 18.74 % mass loss at 3 days and 36.65 % mass loss at 7 days, demonstrating a steady biodegradation rate (Fig. 7e) [62]. The acellular myocardial scaffolds also showed capability to attract and trap water, with a measured water content of 90.21 $\pm$ 2.36 % that was higher than the water content of native myocardium (77.99 $\pm$ 0.46 %) (Fig. 7d).

3.3 Tensile and shear properties of the acellular myocardial scaffolds

Tensile mechanical behavior of the acellular myocardial scaffolds along both PD and XD directions is shown in Fig. 8. Listed in Table 2 are maximum tensile modulus, failure stress, failure strain, and hysteresis of the acellular myocardial scaffolds along PD and XD directions. We found that tensile mechanical behavior along PD direction was significantly stiffer than the XD direction (Fig. 8a; Table 2). The acellular myocardial scaffolds showed much stiffer tensile properties when comparing with the native myocardium [45]. Moreover, the energy dissipation of the acellular myocardial scaffolds was in the range of collagenous tissues [63]. Unlike the differences observed in tensile behavior, the acellular myocardial scaffolds exhibited a weaker shear resistance (shear modulus at 40 % strain: 5.16 $\pm$ 1.35 kPa), which was 8 times lower than the

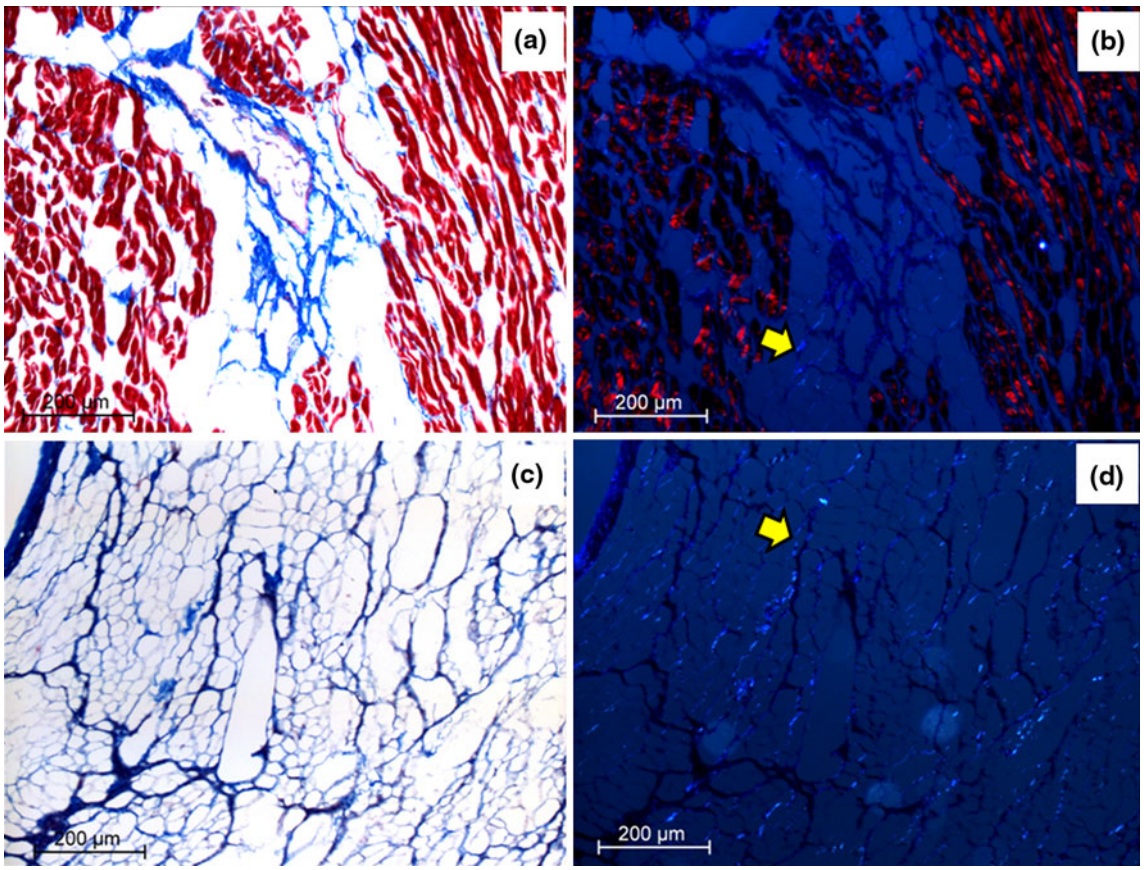

Fig. 4 In polarizing light images, light extinguishing phenomenon of collagen network exists in both the native myocardium (**a**) and the acellular myocardial scaffolds (**b**). The light extinguishing phenomenon reflects collagen wavy pathways

native myocardium (shear modulus at 40 % strain: 42.99 ± 5.79 kPa) (Fig. 8b, c).

4 Discussion

In this study, we thoroughly characterized the acellular porcine myocardial scaffolds that were generated via a modified decellularization procedure. We found that the frame-pin supporting system well preserved 3D cardiomyocyte lacunae, which were clearly confirmed by the cross-sectional and longitudinal views of histology (Fig. 2) and topographic views of SEM (Fig. 3c, d). The pore size of the acellular myocardial scaffolds measured from SEM images showed a radius of 21.4 ± 16.8 μm, which was slightly larger than the pore size (19.5 ± 17.9 μm) reported in our previous study [45]. We had speculated that the capability of acellular myocardial scaffolds being able to maintain open pores is due to the inherent properties of myocardial ECM [45]. In the modified decellularization protocol, the pores might be better maintained open using the frame-pin support system. The quantification of the dimensional changes before and after decellularization showed the overall maintenance of tissue volume, adding more evidence confirming the internal structural preservation (Fig. 7; Table 1).

Another interesting feature revealed by our SEM study is the interconnecting openings inside the cardiomyocyte lacunae (highlighted by arrows in Fig. 3d). Those interconnecting passages were likely an important feature allowing continuity of cardiac muscle fibers both physically and functionally. As reported previously, each ventricular myocyte is connected to other myocytes (via gap junctions), with an average of 11.3 neighbors, 5.3 on the sides and 6.0 at the ends [64]. The preservation of those subtle interconnecting openings in the cardiomyocyte lacunae (Fig. 3d) might benefit not only migration of the reseeded cells in tissue engineering maneuver, but also the possible functional interaction of those cells. Note that the 3D topographic views of cardiac ECM shown in Fig. 3c and d was remarkably similar to a ultrastructural study by Macchiarelli and Ohtani, in which they revealed the lacuna morphology in the NaOH-digested ventricle with SEM [54].

Using polarizing light microscopy, we showed the existence of light extinguishing phenomenon in the collagen network of the native myocardium, while there was no

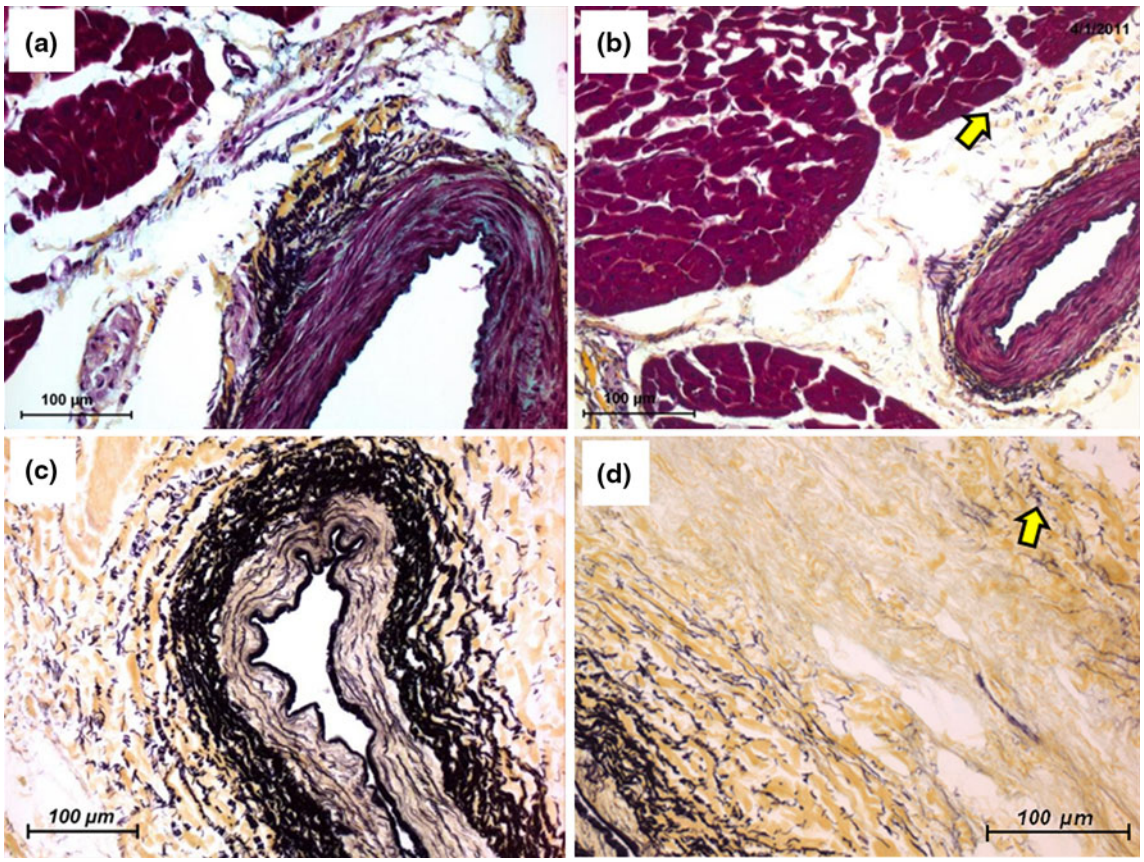

Fig. 5 **a**, **b** Movat's pentachrome staining of the native myocardium, **c**, **d** Movat's pentachrome staining of the acellular myocardial scaffolds. Details of cardiac elastin and vascular elastin were revealed; cardiac elastin is highlighted by arrows. *Yellow* collagen, *Red* cardiomyocytes/smooth muscle cells, *black* elastin, *blue* proteoglycans/glycosaminoglycans (Color figure online)

regular light extinguishing pattern as that shown in tendon or ligament [65]. As we know, the light extinguishing phenomenon under polarizing light resulted from the wavy pathways of collagen fiber bundles (collagen crimp) and the intrinsic birefringence property of collagen [65]. This observation was consistent with Hanley et al.'s finding, which reported that collagen fibers in the native myocardium were wavy cords that were straightened considerably as the sarcomere length was increased from 1.85 ± 0.06 µm (near-resting length) to 2.30 ± 0.04 µm [66]. The retaining of light extinguishing phenomenon in the acellular myocardial scaffolds revealed the preservation of collagen waviness, which suggests a likely beneficial feature for future scaffold-cardiomyocyte interaction and functioning.

An important persevered feature we confirmed in this study was cardiac elastin and elastin in cardiac blood vessels (black color in Movat's Pentachrome staining, Fig. 5). Fomovsky et al., recently pointed out that the myocardium contains collagen, cardiac elastin, proteoglycans, in which the mechanical contributions of cardiac elastin and proteoglycans are relatively poorly understood, and circumferential evidence suggests the need to better understand their mechanical roles [67]. It was well-known that, in other dynamic tissues such as tendon/ligament, heart valves, and blood vessels, elastin fibers/sheets provide resilience by storing and releasing energy in favor of passive recoil (elasticity) [65]. One possible mechanical role of cardiac elastin might be similar to the above mentioned dynamic tissues, i.e., assisting the cardiac contraction cycles by providing microscale resilience. There might be other functions still unknown about cardiac elastin; however, the existence of the cardiac elastin in the native myocardium is a self-evidence of importance from the structure–function point of view. The preservation of cardiac elastin in the acellular myocardial scaffolds hence represents an advantage in biomechanical functionality. Furthermore, the retaining of vascular elastin in blood vessel networks also provides a favorable platform for later revascularization. The conservation of elastin alignment and distribution in the medial layer and the retaining of elastin lamina on the intimal surface might provide important structural cues for smooth muscle cell differentiation and vascular channel endothelialization, respectively.

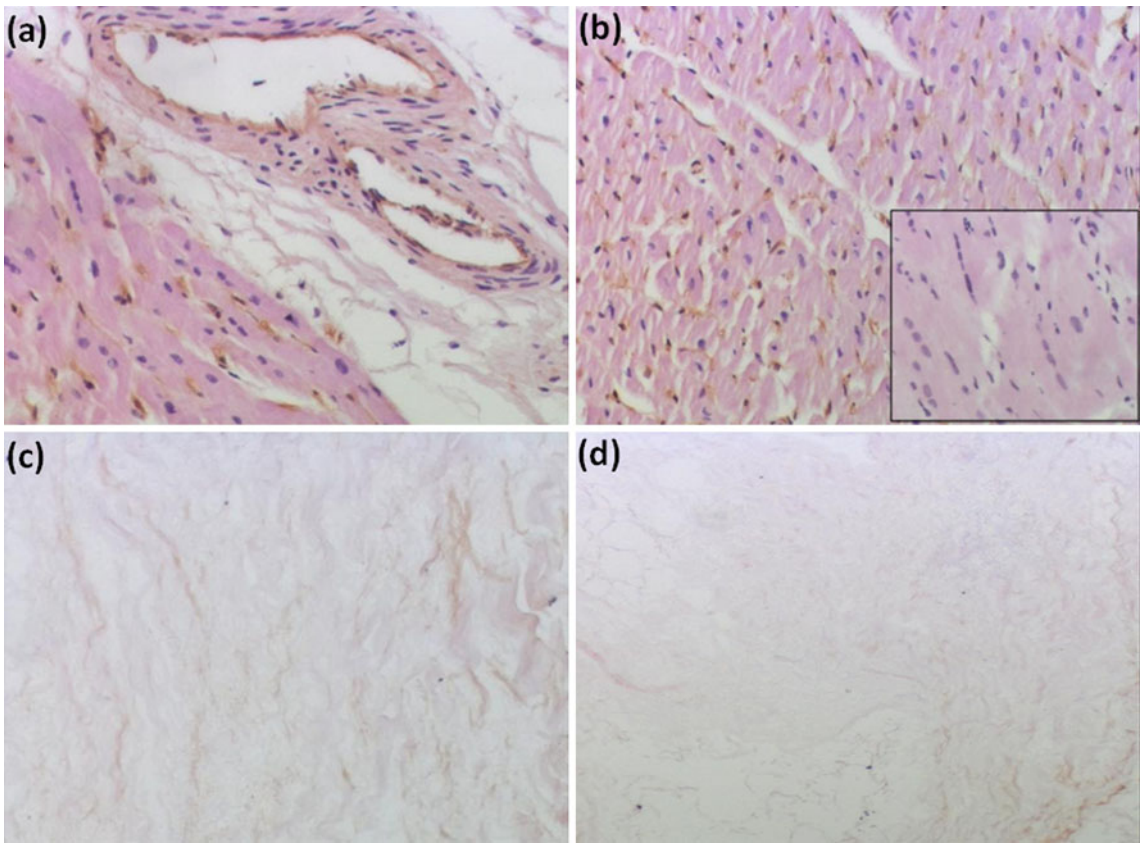

Fig. 6 Histochemical staining for α-Gal. **a**, **b** Native porcine myocardium showed that α-Gal antigen (*brown* color) was associated with myocardial fibroblasts, cardiomyocytes and blood vessels; *inset* shows a negative control where lectin was omitted. **c**, **d** Acellular myocardial scaffolds showed complete lack of staining for the α-Gal antigen (Color figure online)

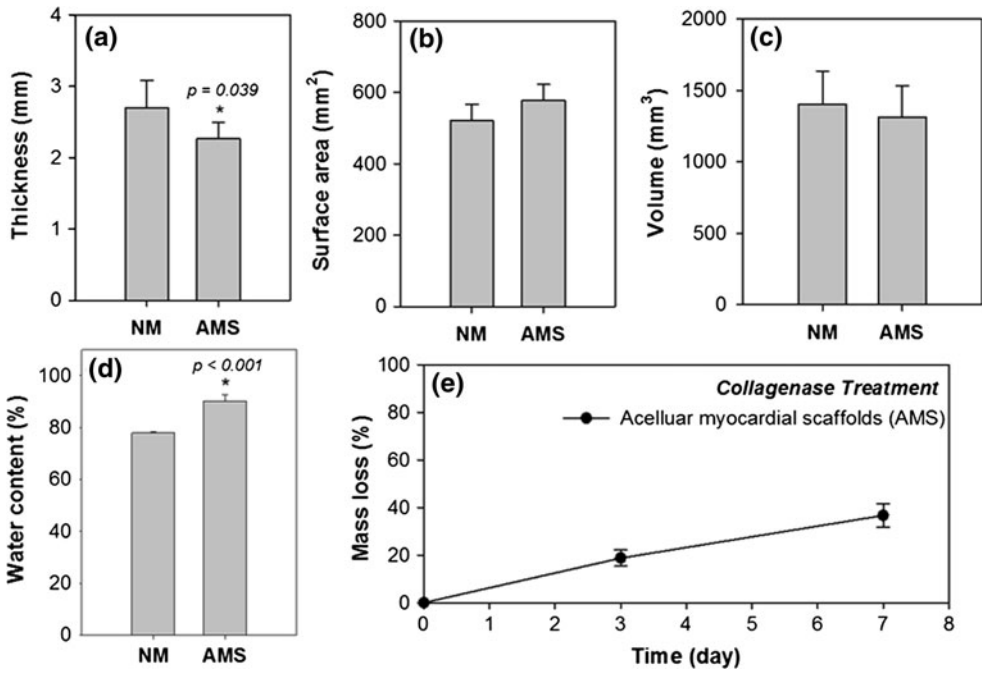

Fig. 7 The dimensional comparison of myocardium samples before and after decellularization: **a** thickness, **b** surface area, and **c** volume. **d** Water content of the native myocardium and the acellular myocardial scaffolds. **e** Mass loss of the acellular myocardial scaffolds at 3 and 7 days in response to collagenase treatment

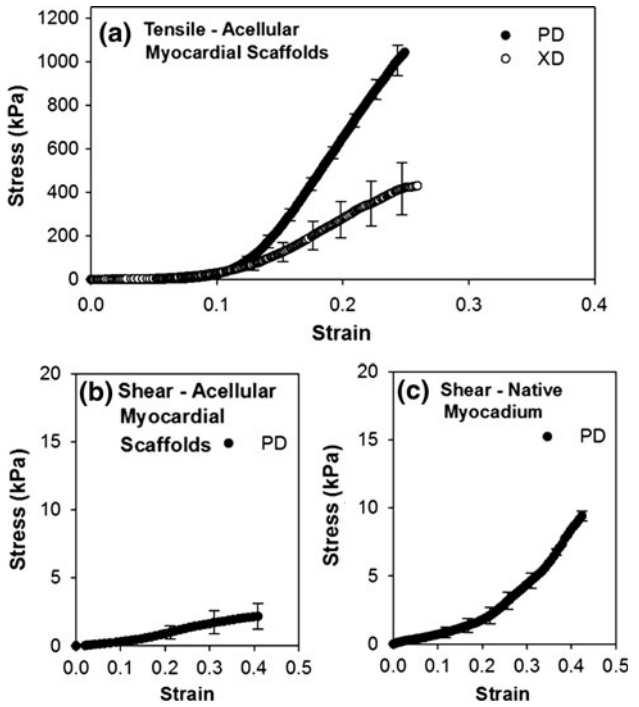

Fig. 8 **a** Uniaxial tensile responses of the acellular myocardial scaffolds along PD and XD directions; samples were loaded up to failure. Shear mechanical responses of the acellular myocardial scaffolds (**b**) and the native myocardium (**c**); only PD direction was examined in shear testing

The efficient removal of cardiomyocytes has been demonstrated histologically by Mason's trichrome staining (Fig. 2). Movat's pentachrome staining (Fig. 5) further showed that smooth muscle cells and endothelial layer in blood vessels were completely removed. Quantitative DNA analysis showed a 98.59 % reduction in DNA content, which was considered satisfactory for tissue engineering applications and comparable to other decellularization studies [68]. α-Gal antigen staining revealed that the acellular myocardial scaffolds completely lacked α-Gal antigen (Fig. 6). The removal of all types of cells, DNA fragments, and α-Gal porcine antigen implied the great potential of the scaffolds in future cardiac regeneration applications.

The water content of decellularized myocardial scaffolds was found higher than the native myocardium (AMS vs. NM: 90.21 ± 2.36 vs. 77.99 ± 0.46 %), reflecting a highly hydrophilic property of the acellular myocardial scaffolds. The high porosity of the acellular scaffolds explained the capability of the acellular scaffolds to attract and trap significant amounts of water. In the accelerating enzymatic degradation assay, we found that the decellularization treatment generated acellular myocardial scaffolds that were biodegradable and had a constant degradation rate (18.74 ± 3.44 % at 3 days and 36.65 ± 4.95 % at 7 days), which is similar to the mass loss in the PGG-fixed porcine pericardium and favors tissue remodeling in the recellularization phase [69, 62].

As we determined in our previous study [45], the stiffer mechanical behavior of the acellular myocardial scaffolds reflected the fact that the decellularization procedure turned a muscular tissue into scaffolds mainly consisting of collagen and elastin networks. The loss of shear resistance in the acellular myocardial scaffolds can be attributed to the highly porous structure. Ideally, for either patch application or whole heart tissue engineering, the passive mechanical properties should be re-established to a certain degree by refilling the empty niches of the acellular myocardial scaffolds with appropriate types of cells. Two efforts are needed in restoration of the passive mechanics of myocardium: one is to lower the tensile properties by adding back cellular contents (matching the patch region with other part of the ventricle) and another is to re-establish shear resistance back to a physiological level. Recellularization and formation of cell-ECM interaction might help re-establish mechanical properties. As we showed in our previous study [45], recellularization promotes positive tissue remodeling and generated patch materials that are more mechanically similar to the native myocardium.

In short, the mechanical and structural parameters, such as tensile and shear properties, pore size of ECM lacunae, etc., were reported here for the acellular myocardial ECM. From a biomimetic point of view, those characteristics might indicate useful mechanical and structural cues for functionality of cardiomyocytes. It is possible that cardiac scaffold design by polymeric or other approaches would be benefited by mimicking the physical and ultrastructural features reported in this study [70]. As an example, a biomaterial scaffold that has very low modulus might not

Table 2 Mechanical parameters obtained from uniaxial tensile testing

Acellular myocardial scaffolds	Maximum tensile modulus (kPa)	Tensile failure stress (kPa)	Tensile failure strain (%)	Hysteresis (%)
Fiber-preferred direction (PD)	9,498.3 ± 1,496.2	1,204.5 ± 40.8	24.99 ± 2.93	10.96 ± 0.37
Cross fiber-preferred direction (XD)	3,270.2 ± 797.8*	333.9 ± 76.2*	25.92 ± 3.47	12.54 ± 1.94
P value	$P = 0.006$	$P < 0.001$	$P = 0.781$	$P = 0.231$

* Indicates statistically significant difference between two groups ($P < 0.05$)

be able to effectively transfer the contractile forces of cardiomyocytes. The future study will include biochemical characterizations of the ECM compositions, biological factors, and ligand integrity in the acellular myocardial scaffolds. It is also worthy to point out that the structural and biomechanical properties reported here are the characteristics of the remaining myocardial scaffolds after decellularization, which are prone to changes in the tissue remodeling processes either in in vitro recellularization/conditioning, or after implantation.

5 Conclusions

We modified the decellularization protocol [45] by employing a frame-pin supporting system, and obtained the acellular myocardial scaffolds that preserved subtle components and features. The aligned and interconnected myocardial niches provide nature-designed microenvironments for future recellularization. The preservation of collagen network, cardiac elastin, and vascular templates further confirmed the potential of porcine myocardial ECM as scaffolds for cardiac tissue engineering/regeneration. We demonstrated the removal of cells, DNA fragments, and α-Gal porcine antigens as well as a constant biodegradation rate rendered by our decellularization procedure. Tensile and shear properties of the acellular myocardial scaffolds were also reported here, together with structural parameters, providing useful information to porcine myocardial ECM and corresponding tissue engineering efforts (e.g., cardiac patch and whole heart tissue engineering).

Acknowledgments This study is supported by NIH National Heart, Lung, and Blood Institute grant HL097321. The authors also would like acknowledge the support from Health Resources and Services Administration (HRSA) (DHHS R1CRH10429-01-00) and the MAFES Strategic Research Initiative Funding (CRESS MIS-741110). The authors thank William Monroe and Amanda Lawrence (MSU EM center) for help on SEM imaging. Support from Sansing Meat Service (Maben, MS) is also greatly appreciated.

References

1. Rosamond W, Flegal K, Friday G, Furie K, Go A, Greenlund K, et al. Heart disease and stroke statistics-2007 update: a report from the American Heart Association Statistics Committee and Stroke Statistics Subcommittee. Circulation. 2007;115(5):e69–171. doi:CIRCULATIONAHA.106.179918,10.1161/CIRCULATIONAHA.106.179918.
2. Takemura G, Ohno M, Hayakawa Y, Misao J, Kanoh M, Ohno A, et al. Role of apoptosis in the disappearance of infiltrated and proliferated interstitial cells after myocardial infarction. Circ Res. 1998;82(11):1130–8.
3. Sun Y, Weber KT. Infarct scar: a dynamic tissue. Cardiovasc Res. 2000;46(2):250–6. doi:S0008-6363(00)00032-8.
4. Kelly D, Khan S, Cockerill G, Ng LL, Thompson M, Samani NJ et al. Circulating stromelysin-1 (MMP-3): a novel predictor of LV dysfunction, remodelling and all-cause mortality after acute myocardial infarction. Eur J Heart Fail. 2008;10(2):133–9. doi:10.1016/j.ejheart.2007.12.009.
5. Sharma R, Raghubir R. Stem cell therapy: a hope for dying hearts. Stem Cells Dev. 2007;16(4):517–36.
6. Losordo DW, Vale PR, Symes JF, Dunnington CH, Esakof DD, Maysky M, et al. Gene therapy for myocardial angiogenesis: initial clinical results with direct myocardial injection of phVEGF165 as sole therapy for myocardial ischemia. Circulation. 1998;98(25):2800–4.
7. Grauss RW, Winter EM, van Tuyn J, Pijnappels DA, Steijn RV, Hogers B, et al. Mesenchymal stem cells from ischemic heart disease patients improve left ventricular function after acute myocardial infarction. Am J Physiol. 2007;293(4):H2438–47.
8. Strauer BE, Kornowski R. Stem cell therapy in perspective. Circulation. 2003;107(7):929–34.
9. Kellar RS, Shepherd BR, Larson DF, Naughton GK, Williams SK. Cardiac patch constructed from human fibroblasts attenuates reduction in cardiac function after acute infarct. Tissue Eng. 2005;11(11–12):1678–87.
10. Barandon L, Couffinhal T, Dufourcq P, Alzieu P, Daret D, Deville C, et al. Repair of myocardial infarction by epicardial deposition of bone-marrow-cell-coated muscle patch in a murine model. Ann Thorac Surg. 2004;78(4):1409–17.
11. Aboulafia-Etzion S, Leor J, Barbash IM, Battler A. Fixing a failing heart: molecular and cellular approaches. Harefuah. 1999;136(4):284–8.
12. Langer R, Vacanti JP. Tissue engineering. Science. 1993;260:920–6.
13. Zimmermann WH, Melnychenko I, Eschenhagen T. Engineered heart tissue for regeneration of diseased hearts. Biomaterials. 2004;25(9):1639–47.
14. Thompson RB, Emani SM, Davis BH, van den Bos EJ, Morimoto Y, Craig D et al. Comparison of intracardiac cell transplantation: autologous skeletal myoblasts versus bone marrow cells. Circulation. 2003;108 Suppl 1:II264–71.
15. Bursac N, Papadaki M, Cohen RJ, Schoen FJ, Eisenberg SR, Carrier R, et al. Cardiac muscle tissue engineering: toward an in vitro model for electrophysiological studies. Am J Physiol. 1999;277(2 Pt 2):H433–44.
16. Carrier RL, Papadaki M, Rupnick M, Schoen FJ, Bursac N, Langer R, et al. Cardiac tissue engineering: cell seeding, cultivation parameters, and tissue construct characterization. Biotechnol Bioeng. 1999;64(5):580–9.
17. Birla RK, Borschel GH, Dennis RG, Brown DL. Myocardial engineering in vivo: formation and characterization of contractile, vascularized three-dimensional cardiac tissue. Tissue Eng. 2005;11(5–6):803–13.
18. Birla RK, Borschel GH, Dennis RG. In vivo conditioning of tissue-engineered heart muscle improves contractile performance. Artif Organs. 2005;29(11):866–75.
19. Borschel GH, Dow DE, Dennis RG, Brown DL. Tissue-engineered axially vascularized contractile skeletal muscle. Plast Reconstr Surg. 2006;117(7):2235–42.
20. Vouyouka AG, Powell RJ, Ricotta J, Chen H, Dudrick DJ, Sawmiller CJ, et al. Ambient pulsatile pressure modulates endothelial cell proliferation. J Mol Cell Cardiol. 1998;30(3):609–15.
21. Fujimoto KL, Guan J, Oshima H, Sakai T, Wagner WR. In vivo evaluation of a porous, elastic, biodegradable patch for reconstructive cardiac procedures. The Annals of thoracic surgery. 2007;83(2):648–54. doi:10.1016/j.athoracsur.2006.06.085.
22. Fujimoto KL, Tobita K, Merryman WD, Guan J, Momoi N, Stolz DB, et al. An elastic, biodegradable cardiac patch induces

contractile smooth muscle and improves cardiac remodeling and function in subacute myocardial infarction. J Am Coll Cardiol. 2007;49(23):2292–300.
23. Li WJ, Laurencin CT, Caterson EJ, Tuan RS, Ko FK. Electrospun nanofibrous structure: a novel scaffold for tissue engineering. J Biomed Mater Res. 2002;60(4):613–21. doi:10.1002/jbm.10167.
24. Smith IO, Liu XH, Smith LA, Ma PX. Nanostructured polymer scaffolds for tissue engineering and regenerative medicine. Wiley Interdiscip Rev Nanomed Nanobiotechnol. 2009;1(2):226–36. doi:10.1002/wnan.26.
25. Ozawa T, Mickle DA, Weisel RD, Koyama N, Wong H, Ozawa S, et al. Histologic changes of nonbiodegradable and biodegradable biomaterials used to repair right ventricular heart defects in rats. J Thorac Cardiovasc Surg. 2002;124(6):1157–64.
26. Ozawa T, Mickle DA, Weisel RD, Koyama N, Ozawa S, Li RK. Optimal biomaterial for creation of autologous cardiac grafts. Circulation. 2002;106(12 Suppl 1):I176–82.
27. Engelmayr GC Jr, Cheng M, Bettinger CJ, Borenstein JT, Langer R, Freed LE. Accordion-like honeycombs for tissue engineering of cardiac anisotropy. Nat Mater. 2008;7(12):1003–10.
28. Hutmacher DW, Goh JC, Teoh SH. An introduction to biodegradable materials for tissue engineering applications. Ann Acad Med Singap. 2001;30(2):183–91.
29. Hutmacher DW. Scaffold design and fabrication technologies for engineering tissues—state of the art and future perspectives. J Biomater Sci Polym Ed. 2001;12(1):107–24.
30. Grad S, Zhou L, Gogolewski S, Alini M. Chondrocytes seeded onto poly (L/DL-lactide) 80/20% porous scaffolds: a biochemical evaluation. J Biomed Mater Res A. 2003;66(3):571–9. doi:10.1002/jbm.a.10007.
31. Weber B, Emmert MY, Schoenauer R, Brokopp C, Baumgartner L, Hoerstrup SP. Tissue engineering on matrix: future of autologous tissue replacement. Semin Immunopathol 33(3):307–15. doi:10.1007/s00281-011-0258-8.
32. Hodde J. Naturally occurring scaffolds for soft tissue repair and regeneration. Tissue Eng. 2002;8(2):295–308. doi:10.1089/107632702753725058.
33. Atala A, Bauer SB, Soker S, Yoo JJ, Retik AB. Tissue-engineered autologous bladders for patients needing cystoplasty. Lancet. 2006;367(9518):1241–6. doi:10.1016/S0140-6736(06)68438-9.
34. Wang X, Lin P, Yao Q, Chen C. Development of small-diameter vascular grafts. World J Surg. 2007;31(4):682–9. doi:10.1007/s00268-006-0731-z.
35. Gilbert TW, Sellaro TL, Badylak SF. Decellularization of tissues and organs. Biomaterials. 2006;27(19):3675–83.
36. Liao J, Joyce EM, Sacks MS. Effects of decellularization on mechanical and structural properties of the porcine aortic valve leaflets. Biomaterials. 2008;29(8):1065–74.
37. Borschel GH, Huang YC, Calve S, Arruda EM, Lynch JB, Dow DE, et al. Tissue engineering of recellularized small-diameter vascular grafts. Tissue Eng. 2005;11(5–6):778–86.
38. Borschel GH, Dennis RG, Kuzon WM, Jr. Contractile skeletal muscle tissue-engineered on an acellular scaffold. Plastic Reconstr Surg. 2004;113(2):595–602 (discussion 3–4).
39. Badylak SF, Tullius R, Kokini K, Shelbourne KD, Klootwyk T, Voytik SL, et al. The use of xenogeneic small intestinal submucosa as a biomaterial for Achilles tendon repair in a dog model. J Biomed Mater Res. 1995;29(8):977–85.
40. Leor J, Aboulafia-Etzion S, Dar A, Shapiro L, Barbash IM, Battler A et al. Bioengineered cardiac grafts: a new approach to repair the infarcted myocardium? Circulation 2000;102(19 Suppl 3):III56–61.
41. Badylak SF. Xenogeneic extracellular matrix as a scaffold for tissue reconstruction. Transpl Immunol 2004;12(3–4):367–77. doi:10.1016/j.trim.2003.12.016.
42. Hoshiba T, Lu H, Kawazoe N, Chen G. Decellularized matrices for tissue engineering. Expert Opin Biol Ther 10(12):1717–28. doi:10.1517/14712598.2010.534079.
43. Knight RL, Wilcox HE, Korossis SA, Fisher J, Ingham E. The use of acellular matrices for the tissue engineering of cardiac valves. Proc Inst Mech Eng H. 2008;222(1):129–43.
44. Ott HC, Matthiesen TS, Goh SK, Black LD, Kren SM, Netoff TI, et al. Perfusion-decellularized matrix: using nature's platform to engineer a bioartificial heart. Nat Med. 2008;14(2):213–21.
45. Wang B, Borazjani A, Tahai M, Curry AL, Simionescu DT, Guan J et al. Fabrication of cardiac patch with decellularized porcine myocardial scaffold and bone marrow mononuclear cells. J Biomed Mater Res A 94(4):1100–10. doi:10.1002/jbm.a.32781.
46. Godier-Furnemont AF, Martens TP, Koeckert MS, Wan L, Parks J, Arai K et al. Composite scaffold provides a cell delivery platform for cardiovascular repair. Proc Natl Acad Sci USA 108(19):7974–9.
47. Badylak SF, Taylor D, Uygun K. Whole-organ tissue engineering: decellularization and recellularization of three-dimensional matrix scaffolds. Ann Review Biomed Eng 13:27–53.
48. Wainwright JM, Czajka CA, Patel UB, Freytes DO, Tobita K, Gilbert TW et al. Preparation of cardiac extracellular matrix from an intact porcine heart. Tissue Eng Part C Methods. 2010;16(3):525–32.
49. Crapo PM, Gilbert TW, Badylak SF. An overview of tissue and whole organ decellularization processes. Biomaterials. 2011;32(12):3233–43.
50. Witzenburg C, Raghupathy R, Kren SM, Taylor DA, Barocas VH. Mechanical changes in the rat right ventricle with decellularization. J Biomech.
51. Streeter D, Powers WE, Ross A, Torrent-Guasp F. Three-Dimensional Fiber Orientation in the Mammalian Left Ventricular Wall. Cardiovascular System Dynamics. Cambridge: M.I.T Press; 1978. p. 73.
52. Streeter DD Jr, Hanna WT. Engineering mechanics for successive states in canine left ventricular myocardium. II. Fiber angle and sarcomere length. Circ Res. 1973;33(6):656–64.
53. Streeter DD Jr, Spotnitz HM, Patel DP, Ross J Jr, Sonnenblick EH. Fiber orientation in the canine left ventricle during diastole and systole. Circ Res. 1969;24(3):339–47.
54. Macchiarelli G, Ohtani O. Endomysium in left ventricle. Heart (British Cardiac Society). 2001;86(4):416.
55. Weber KT. Cardiac interstitium in health and disease: the fibrillar collagen network. J Am Coll Cardiol. 1989;13(7):1637–52.
56. Holmes JW, Borg TK, Covell JW. Structure and mechanics of healing myocardial infarcts. Annu Rev Biomed Eng. 2005;7:223–53.
57. Humphery JD. Cardiovascular Solid Mechanics. Berlin: Springer; 2002.
58. Strokan V, Molne J, Svalander CT, Breimer ME. Heterogeneous expression of Gal alpha1-3Gal xenoantigen in pig kidney: a lectin and immunogold electron microscopic study. Transplantation. 1998;66(11):1495–503.
59. Azimzadeh A, Wolf P, Thibaudeau K, Cinqualbre J, Soulillou JP, Anegon I. Comparative study of target antigens for primate xenoreactive natural antibodies in pig and rat endothelial cells. Transplantation. 1997;64(8):1166–74.
60. Tedder ME, Liao J, Weed B, Stabler C, Zhang H, Simionescu A, et al. Stabilized collagen scaffolds for heart valve tissue engineering. Tissue Eng Part A. 2009;15(6):1257–68.
61. Shanmugasundaram N, Ravichandran P, Reddy PN, Ramamurty N, Pal S, Rao KP. Collagen-chitosan polymeric scaffolds for the in vitro culture of human epidermoid carcinoma cells. Biomaterials. 2001;22(14):1943–51. doi:S0142961200002209.
62. Sierad LN, Simionescu A, Albers C, Chen J, Maivelett J, Tedder ME et al. Design and testing of a pulsatile conditioning system

for dynamic endothelialization of polyphenol-stabilized tissue engineered heart valves. Cardiovasc Eng Technol. 2009;1(2): 138–53. doi:10.1007/s13239-010-0014-6.
63. Roeder BA, Kokini K, Sturgis JE, Robinson JP, Voytik-Harbin SL. Tensile mechanical properties of three-dimensional type I collagen extracellular matrices with varied microstructure. J Biomech Eng. 2002;124(2):214–22.
64. Saffitz JE, Kanter HL, Green KG, Tolley TK, Beyer EC. Tissue-specific determinants of anisotropic conduction velocity in canine atrial and ventricular myocardium. Circ Res. 1994;74(6): 1065–70.
65. Fung YC. Biomechanics: mechanical properties of living tissues. New York: Springer; 1981.
66. Hanley PJ, Young AA, LeGrice IJ, Edgar SG, Loiselle DS. 3-Dimensional configuration of perimysial collagen fibres in rat cardiac muscle at resting and extended sarcomere lengths. J Physiol. 1999;517(Pt 3):831–7. doi:PHY_9009.
67. Fomovsky GM, Thomopoulos S, Holmes JW. Contribution of extracellular matrix to the mechanical properties of the heart. J Mol Cell Cardiol. 2010;48(3):490–6. doi:10.1016/j.yjmcc.2009.08.003.
68. Baraki H, Tudorache I, Braun M, Höffler K, Görler A, Lichtenberg A, et al. Orthotopic replacement of the aortic valve with decellularized allograft in a sheep model. Biomaterials. 2009; 30(31):6240–6.
69. Goo HC, Hwang YS, Choi YR, Cho HN, Suh H. Development of collagenase-resistant collagen and its interaction with adult human dermal fibroblasts. Biomaterials. 2003;24(28):5099–113. doi:S0142961203004319.
70. Guan J, Wang F, Li Z, Chen J, Guo X, Liao J et al. The stimulation of the cardiac differentiation of mesenchymal stem cells in tissue constructs that mimic myocardium structure and biomechanics. Biomaterials. 2011;32(24):5568–80. doi:10.1016/j.biomaterials.2011.04.038.